THE JOURNAL OF PROSTHETIC DENTISTRY

RESEARCH AND EDUCATION

Flexural and structural behavior of additively manufactured zirconia: Influence of firing process and build orientation

Gabriela Panca Sabatini, Dr med dent, MSc, PhD,[a] Mustafa Borga Donmez, DDS, PhD,[b] Pedro Molinero-Mourelle, PD, Dr med dent, MAS, PhD,[c] Gülce Çakmak, DDS, Dr med dent, PhD,[d] Mehmet Esad Güven, DDS, PhD,[e] Ahmet Burçin Batıbay, M&ME, PhD,[f] Newton Sesma, DDS, MSc, PhD,[g] and Burak Yilmaz, DDS, PhD[h]

ABSTRACT

Statement of problem. Additive manufacturing of zirconia is gaining popularity in dentistry; however, knowledge of the influence of build orientation and firing process on its mechanical properties and structural behavior remains limited.

Purpose. The purpose of this in vitro study was to compare the effect of firing process and build orientation on the flexural strength (FS) and structural characteristics of additively manufactured 3% mol yttria-stabilized tetragonal zirconia polycrystal (3Y-TZP) with subtractively manufactured 3Y-TZP and 4Y-TZP.

Material and methods. A total of 192 bar-shaped (17×4×1.5 mm) and 16 disk-shaped (Ø10×1.5 mm) specimens were manufactured either additively with a 3Y-TZP slurry (INNI Cera) or subtractively with presintered 3Y-TZP (IPS e.max ZirCAD LT [SM-LT]) or 4Y-TZP (IPS e.max ZirCAD MT [SM-MT]) zirconia disks. The additively manufactured specimens were categorized based on build orientation (0-degree [AMH], 45-degree [AMD], and 90-degree [AMV]) and firing process (combined [1-step] or separate [2-step] debinding and sintering cycle). All specimens were divided into 2 groups (n=12 for bar-shaped and n=1 for disk-shaped specimens) of aged (thermocycling for 10 000 cycles between 5 °C and 55 °C) and nonaged. Bar-shaped specimens were tested for FS, while disk-shaped specimens were used for structural characterization using X-ray diffraction (XRD) and scanning electron microscope (SEM) imaging. The FS data were analyzed with general linear model analysis and Bonferroni-corrected post hoc tests (α=.05).

Results. The interaction between manufacturing protocol and aging condition affected the FS values (*P*<.001). Among the nonaged specimens, SM-LT led to higher FS than AMD-2 and AMV-1, while AMH-1 led to higher FS than AMV-1 (*P*≤.007). Among the aged specimens, AMV resulted in the lowest FS, regardless of the firing process (*P*≤.034). Aging reduced the FS of AMV-2 (*P*<.001). All subgroups showed a dominant tetragonal phase with a detectable monoclinic peak at 51.2-degree, with AMD exhibiting lower peak intensity than AMH and AMV, and SM-LT showing higher tetragonal peak intensity than SM-MT; aging increased localized crystallinity in all subgroups, as evidenced by higher XRD peak intensities. SEM analysis showed that AM specimens exhibited characteristic delineation and residual pores, whereas SM specimens displayed linear milling marks from burs and a higher concentration of monoclinic-phase crystals.

Conclusions. At 0-degree orientation, the tested 3Y-TZP slurry demonstrated load-bearing capacity comparable with that of subtractively manufactured 3Y-TZP and 4Y-TZP, regardless of the firing process. However, SEM analysis of AM specimens revealed residual pores, and SM specimens showed a higher concentration of monoclinic-phase crystals. (J Prosthet Dent 2026;135:612.e1-e8)

The authors declare that they have no known competing financial interests or personal relationships that could have appeared to influence the work reported in this paper.

[a]Clinical Assistant, Department of Reconstructive Dentistry and Gerodontology, School of Dental Medicine, University of Bern, Bern, Switzerland.
[b]Associate Professor, Department of Prosthodontics, Faculty of Dentistry, Biruni University, İstanbul, Turkey; and External Researcher, Department of Reconstructive Dentistry and Gerodontology, School of Dental Medicine, University of Bern, Bern, Switzerland.
[c]Senior Lecturer, Department of Reconstructive Dentistry and Gerodontology, School of Dental Medicine, University of Bern, Bern, Switzerland; and Senior Lecturer, Department of Conservative Dentistry and Prosthodontics, Faculty of Complutense University of Madrid, Ramon y Cajal Research Institute (IRYCIS), Madrid, Spain.
[d]Senior Research Associate, Department of Reconstructive Dentistry and Gerodontology, School of Dental Medicine, University of Bern, Bern, Switzerland; and Head of the Digital Dental Technology Laboratory, Department of Prosthodontics, Geriatric Dentistry and Craniomandibular Disorders, Charité Universitätsmedizin Berlin, Corporate Member of Freie Universität Berlin and Humboldt-Universität zu Berlin, Berlin, Germany; and External Researcher, Department of Prosthodontics, Faculty of Dentistry, Biruni University, İstanbul, Turkey.
[e]Associate Professor, Department of Prosthodontics, Faculty of Dentistry, Necmettin Erbakan University, Konya, Turkey.
[f]Senior Engineer, R&D and Technology Directorate, Mechanical and Chemical Industry Corporation, Ankara, Turkey.
[g]Associate Professor, Department of Prosthodontics, School of Dentistry, University of São Paulo (USP), São Paulo, Brazil.
[h]Professor, Department of Reconstructive Dentistry and Gerodontology, School of Dental Medicine, University of Bern, Bern, Switzerland; Professor, Department of Restorative, Preventive and Pediatric Dentistry, School of Dental Medicine, University of Bern, Bern, Switzerland; Adjunct Professor, Division of Restorative and Prosthetic Dentistry, The Ohio State University, Columbus, Ohio; and Adjunct Professor, Department of Prosthodontics, Faculty of Dentistry, Ankara University, Ankara, Turkey.

Clinical Implications

Tested 3Y-TZP slurry exhibited flexural strength comparable with that of subtractively manufactured 3Y-TZP and 4Y-TZP, supporting its use in short-span prostheses across groups and in long-span prostheses when printed at 0-degree orientation and processed with separate debinding and sintering. SEM analysis revealed a more porous microstructure in additively manufactured specimens, which warrants further investigation regarding possible effects on long-term performance. In subtractively manufactured groups, XRD indicated higher monoclinic content after aging, suggesting the need for further evaluation of their susceptibility to low-temperature degradation.

Digital technologies are transforming dentistry through high-resolution imaging and the widespread use of computer-aided design and computer-aided manufacturing (CAD-CAM) systems.[1] Both additive (AM) and subtractive (SM) manufacturing have enhanced the efficiency of prosthesis fabrication, improving clinical workflows and patient comfort.[2] These technologies enable the use of zirconia, a polycrystalline material with monoclinic, tetragonal, and cubic phases,[3,4] valued for its mechanical strength and esthetic properties.[5–9] Zirconia has been further classified based on yttria content, such as 3 mol% or 4 mol% yttria-stabilized tetragonal zirconia polycrystal (3Y-TZP and 4Y-TZP).[10,11] However, SM of zirconia has drawbacks, including limited ability to fabricate complex hollow geometries, high material waste, and risk of surface microcracks from bur vibration or overmilling.[12–16] The AM of zirconia addresses several of these limitations by enabling large-scale production, minimizing material waste, and allowing the fabrication of complex geometries with fine details.[17,18]

Vat polymerization-based AM technologies, in which objects are fabricated from a photopolymerizable resin matrix containing dispersed ceramic particles,[10,19] have been commonly used for zirconia.[6,14,16,19–22] Although essential, the resin matrix requires debinding to remove the organic binder, followed by sintering to achieve final density and properties.[23–26] The firing process can follow either a 1-step or 2-step approach.[27] In the 1-step approach, debinding is immediately followed by sintering without cooling to room temperature, significantly shortening postprocessing time and potentially facilitating a more efficient workflow. In contrast, the 2-step process completes debinding, allows the material to cool, and then performs high-temperature sintering, which also enables the internal staining of zirconia to enhance esthetics.[17,21] Regardless of the firing process, build orientation may affect the properties of additively manufactured zirconia,[16,21,24,28,29] considering its anisotropic behavior.[1,30]

Understanding how build orientation and firing processes influence flexural properties and structural behavior is essential for clinicians and dental laboratory technicians to implement this technology safely and effectively, particularly as the use of additively manufactured zirconia for various prosthetic restorations continues to rise[9,12,13] and as a recent study has highlighted the significant combined effects of these factors.[27] While previous research has examined the individual influence of firing process or build orientation on the flexural strength (FS) and structural properties of additively manufactured zirconia,[1,15–17,19,24,28,30–32] knowledge regarding their combined impact, including changes induced by aging, remains limited.[21] The mechanical and structural behavior of zirconia is influenced not only by the manufacturing process[20,26] but also by aging, which can induce tetragonal-to-monoclinic transformation, alter grain boundaries and porosity, and thereby affect mechanical performance and long-term reliability.[11] Therefore, this study aimed to compare the FS and structural characteristics of additively manufactured 3Y-TZP zirconia with those of subtractively manufactured 3Y-TZP and 4Y-TZP zirconia, considering different build orientations and firing protocols and to assess the impact of thermal aging on these properties. The null hypothesis was that the manufacturing protocol, whether additively manufactured with different firing processes and build orientations or subtractively manufactured from disks with different yttria contents, and the aging condition would not affect the flexural strength or structural properties of the tested zirconia materials.

MATERIAL AND METHODS

Sample size per group was determined through a power analysis (α=.05, 1-β=.95, effect size f=1.56) using the results of a pilot study which indicated that 4 specimens per group would be sufficient. However, to enhance statistical reliability and account for potential specimen loss during testing, 12 specimens were fabricated for each group. Table 1 provides detailed information on the tested materials.

For the FS tests, a bar-shaped standard tessellation language (STL) file (17×4×1.5 mm) was designed using a CAD software program (Meshmixer v3.5.474; Autodesk Inc) and imported into the nesting software program (ZiproS v3.1.106; AON) of a digital light processing-based 3D printer (KUAIPRINT; Manfredi). The STL file was oriented at 0 degrees (AMH), 45 degrees (AMD), or 90 degrees (AMV), with a separate nesting file for each, where at 0 degrees the specimens were positioned with their wide surface (17×4 mm) facing the build platform,

Table 1. Detailed information on test groups

Group Name	Material	Chemical Composition (wt%)	Manufacturing Method
AMH–1 AMH–2 AMD–1 AMD–2 AMV–1 AMV–2	INNI Cera BCM-W1000	ZrO_2: 92.5% Y_2O_3: 4.67% HfO_2: 1.64% Al_2O_3: 0.07% Other oxides:<2.0%	Additively manufactured with 0-degree build orientation, 1-step firing Additively manufactured with 0-degree build orientation, 2-step firing Additively manufactured with 45-degree build orientation, 1-step firing Additively manufactured with 45-degree build orientation, 2-step firing Additively manufactured with 90-degree build orientation, 1-step firing Additively manufactured with 90-degree build orientation, 2-step firing
SM-LT	IPS e.max ZirCAD LT	ZrO_2: 88.0–95.5% Y_2O_3: >4.5% – ≤6.0% HfO_2: ≤5.0% Al_2O_3: ≤1.0% Other oxides: ≤1.0%	Subtractively manufactured
SM-MT	IPS e.max ZirCAD MT	ZrO_2: 86.0–93.5% Y_2O_3: >6.5% – ≤8.0% HfO_2: ≤5.0% Al_2O_3: ≤1.0% Other oxides: ≤1.0%	

Chemical compositions were obtained from the respective manufacturer technical sheets.

at 90 degrees with their narrow surface (17×1.5 mm) facing it, and at 45 degree with an intermediate tilt between these extremes. Support structures were generated automatically, and each design was duplicated until 12 specimens were positioned on the build platform. Fabrication was performed using a 3Y-TZP zirconia slurry (INNI Cera BCM W1000; AON), with each build based on a nesting file containing 12 duplicated STL specimens in the same orientation, which was printed 4 times to account for both firing protocols and aging conditions. The layer thickness was set at 50 µm. After printing, the specimens were ultrasonically cleaned in isopropyl alcohol for 4 minutes (2 minutes prewash, 2 minutes postwash), with supports manually removed during cleaning, and then left to air dry for 10 minutes. For each build orientation, 1 batch underwent a combined debinding and sintering process (1-step), and the other underwent separate debinding and sintering (2-step), resulting in 6 experimental subgroups: AMH-1 and AMH-2 (0-degree, 1-step and 2-step), AMD-1 and AMD-2 (45-degree, 1-step and 2-step), and AMV-1 and AMV-2 (90-degree, 1-step and 2-step). All AM specimens were sintered in the same furnace (ZYNTAPRINT-S; Manfredi), regardless of the firing process (Table 2). The same STL file was also used to fabricate 24 specimens each from 3Y-TZP (SM-LT, IPS e.max ZirCAD LT; Ivoclar AG) and 4Y-TZP (SM-MT, IPS e.max ZirCAD MT; Ivoclar AG) disks with a 5-axis milling unit (PrograMill PM7; Ivoclar AG) and its associated nesting software program (PrograMill CAM V4.2; Ivoclar AG). After milling, the supporting structures were removed with a bur (ZirconFlex Kit 1322 SZ652R; JOTA AG), and the specimens were sintered in a furnace (Programat S2; Ivoclar AG) according to the manufacturer's recommendations for 9 hours and 50 minutes (Table 3). No additional polishing or glazing was performed on any of the specimens. The same CAD software program was used to design a disk-shaped STL

Table 2. Firing parameters of additively manufactured zirconia specimens

		Start Temperature (°C)	End Temperature (°C)	Rising temperature (°C)	Ramp-up rate (°C/min)	Time (min)
One-step debinding and sintering	1	0	150	150	10	15
	2	150	200	50	5	10
	3	200	320	120	0.2	600
	4	320	320	0	0	60
	5	320	490	170	0.5	340
	6	490	490	0	0	60
	7	490	1500	1010	10	100
	8	1500	1500	0	0	120
Two-step debinding and sintering	Debinding	Start temperature (°C)	End temperature (°C)	Rising temperature (°C)	Ramp-up Rate (°C/min)	Time (min)
	1	0	150	150	10	15
	2	150	200	50	5	10
	3	200	320	120	0.2	600
	4	320	320	0	0	60
	5	320	490	170	0.5	340
	6	490	490	0	0	60
	7	490	1100	610	10	61
	8	1100	1100	0	0	60
	Sintering	**Start temperature (°C)**	**End temperature (°C)**	**Rising temperature (°C)**	**Ramp-up Rate (°C/min)**	**Time (min)**
	1	0	1200	1200	10	120
	2	1200	1500	300	5	60
	3	1500	1500	0	0	120

Table 3. Sintering parameters of subtractively manufactured zirconia specimens

		Start temperature (°C)	End temperature (°C)	Heating/cooling rate (°C)	Holding time (min)
Sintering	1	20	900	10	30
	2	900	1500	3.3	120
	3	1500	900	10	-
	4	900	300	8.3	-

file (Ø10×1.5 mm) to evaluate the effects of firing process and build orientation on the structural properties of AM zirconia. One specimen from each material-aging pair was fabricated and processed for X-ray diffraction (XRD) and scanning electron microscopy (SEM) analyses, as described previously. The dimensions of all specimens adhered to the International Organization for Standardization (ISO) standard 6872:2024.[33]

Following fabrication, specimen dimensions were verified using digital calipers (Model NB60; Mitutoyo American Corp), and each set of bar- and disk-shaped specimens was randomly divided with a spreadsheet (Excel; Microsoft Corp) into 2 subgroups: nonaged and aged. Specimens in the aged subgroups, regardless of shape, underwent thermal aging for 10 000 cycles between 5 °C and 55 °C, with a dwell time of 30 seconds and a transfer time of 10 seconds (SD Mechatronik Thermocycler; SD Mechatronik GmbH), simulating approximately 1 year of intraoral service,[34] while nonaged specimens were stored in an incubator for 24 hours at 37 °C. The nonaged and aged bar-shaped specimens were subjected to a 3-point FS test using a universal testing machine (zwickiLine Z1.0 TN; Zwick-Roell), with a span length of 12 mm and a crosshead speed of 1 mm/minute,[33,35] during which the support-free wide surfaces were positioned under load. FS values were calculated in megapascals (MPa) using the formula $FS=3PL/2wb^2$, where P is the fracture load (N), L is the span length (mm), w is the width (mm), and b is the thickness (mm) of the specimen.[24,36,37]

The support-free surface of the disk-shaped specimens was examined using a diffractometer (Empyrean; Malvern Panalytical Ltd) operated at 45 kV and 40 mA with Cu-Kα radiation (λ=1.5406 Å). Diffractograms were collected over a 2θ range of 10- to 100-degrees (step size 0.013 degrees), and patterns were interpreted by comparing peak positions and intensities with literature data to confirm phase identity.[38,39] The same specimens were examined by SEM (SU1510; Hitachi) at ×500 and ×5000 magnifications to assess surface topography with and without aging. Images were visually inspected to evaluate morphological characteristics, including pores and delamination, as previously described.[39]

The normality of the FS data was assessed using the Shapiro-Wilk test on the residuals, confirming a normal distribution. A general linear model was then applied to evaluate the effects of manufacturing protocol, aging condition (nonaged and aged), and their interaction on FS values. Post hoc comparisons were performed with Bonferroni correction. All statistical analyses were conducted using a software program (Minitab Software V.17; Minitab) (α=.05).

RESULTS

General linear model analysis revealed significant effects of manufacturing protocol (F=15.73, *P*<.001), aging (F=5.54, *P*=.020), and their interaction (F=5.21, *P*<.001) on flexural strength. When the clinically relevant pairs were considered (materials within the same aging condition or aging protocols within the same material), SM-LT showed higher FS than AMD-2 and AMV-1 among the nonaged specimens (*P*≤.007), while AMH-1 showed higher FS than AMV-1 (*P*=.005). Within the aged specimens, AMV exhibited the lowest FS values (*P*≤.034). Aging only reduced the FS of AMV-2 (*P*<.001, Table 4).

Figure 1 displays the XRD patterns of all subgroups. Regardless of the material and aging conditions, the tetragonal phase was predominant in all subgroups. However, the monoclinic phase was also detected. AMD specimens showed lower peak intensities than AMH and AMV specimens, independent of the firing process and aging conditions. The SM-LT specimens exhibited a more pronounced tetragonal peak than both aged and unaged SM-MT specimens, indicating a higher tetragonal phase content than the other subgroups. The XRD results suggested that aging may increase diffraction peak intensity, potentially indicating an enhancement in the crystal characteristics of the material, which may imply an improved lattice arrangement or grain growth.

SEM observations were obtained by visual inspection of representative areas at ×500 and ×5000 magnifications. At ×500 magnification, AMD and AMV specimens

Table 4. Mean ±standard deviation flexural strength values of subgroups (MPa)

	Nonaged	Aged
AMH–1	930 ±200de	765 ±239^{cde}
AMH–2	825 ±202^{cde}	821 ±216^{cde}
AMD–1	786 ±197^{cde}	783 ±119^{cde}
AMD–2	700 ±225^{bcd}	826 ±106^{cde}
AMV–1	654 ±123^{abc}	524 ±91^{ab}
AMV–2	784 ±154^{cde}	449 ±117^{a}
SM-LT	969 ±135^{e}	963 ±105^{e}
SM-MT	853 ±116^{cde}	936 ±85^{e}

Different superscript lowercase letters indicate significant differences among subgroups (*P*<.05)

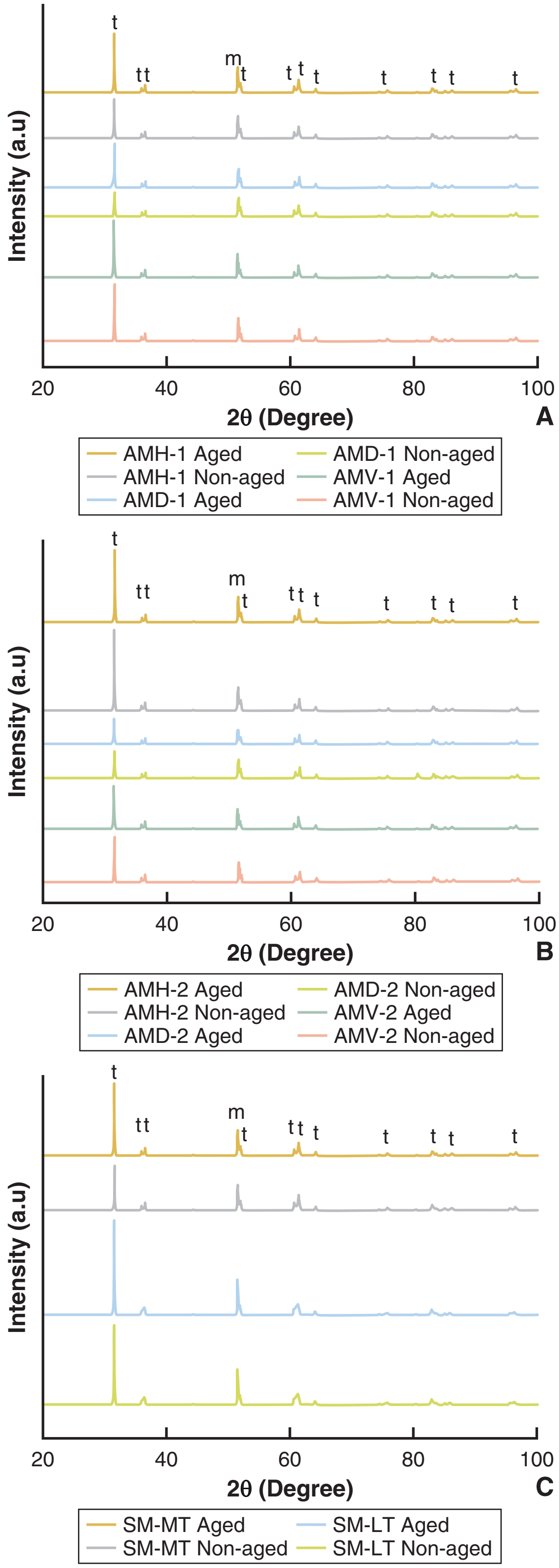

Figure 1. X-ray diffraction patterns of subgroups. AMD-1, Additively manufactured zirconia specimens with 45-degree build orientation and 1-step debinding and sintering; AMD-2, Additively manufactured zirconia specimens with 45-degree build orientation and 2-step debinding and sintering; AMH-1, Additively manufactured zirconia specimens with 0-degree build orientation and 1-step debinding and sintering; AMH-2, Additively manufactured zirconia specimens with 0-degree build orientation and 2-step debinding and sintering; AMV-1, Additively manufactured zirconia specimens with 90-degree build orientation and 1-step debinding and sintering; AMV-2, Additively manufactured zirconia specimens with 90-degree build orientation and 2-step debinding and sintering; SM-LT, IPS e.max ZirCAD LT; SM-MT, IPS e.max ZirCAD MT.

exhibited layering patterns formed during fabrication, independent of firing process or aging conditions. The images of the SM-LT and SM-MT specimens at this magnification were characterized by linear markings, likely resulting from milling tools used during manufacturing. At ×5000, the images of AM specimens displayed small black dots, indicative of the pores remaining from the debinding process, regardless of the firing and aging conditions. Across all subgroups, small white structures interpreted as monoclinic phase zirconia particles were observed in higher concentrations in the SM groups and in all materials after thermal cycling; these microstructural findings after aging aligned with the subtle changes detected by XRD. Delamination and microcracks were also evident in AMD and AMV specimens, irrespective of aging, with AMV-1 specimens showing more pronounced interlayer delamination than AMV-2 specimens under both aging conditions (Fig. 2).

DISCUSSION

The interaction between the manufacturing protocol and aging condition affected the FS of tested specimens. In addition, visible differences were found among the test groups when XRD and SEM findings were considered. Therefore, the null hypotheses that the manufacturing protocol, whether additively manufactured with different firing processes and build orientations or subtractively manufactured from disks with different yttria contents, and the aging condition would not affect the flexural strength or structural properties of the tested zirconia materials were rejected.

The ISO 6872:2024 standard specifies an FS threshold of 300 MPa for monolithic 3-unit prostheses excluding molar teeth, 500 MPa for monolithic 3-unit prostheses involving molar teeth, and 800 MPa for

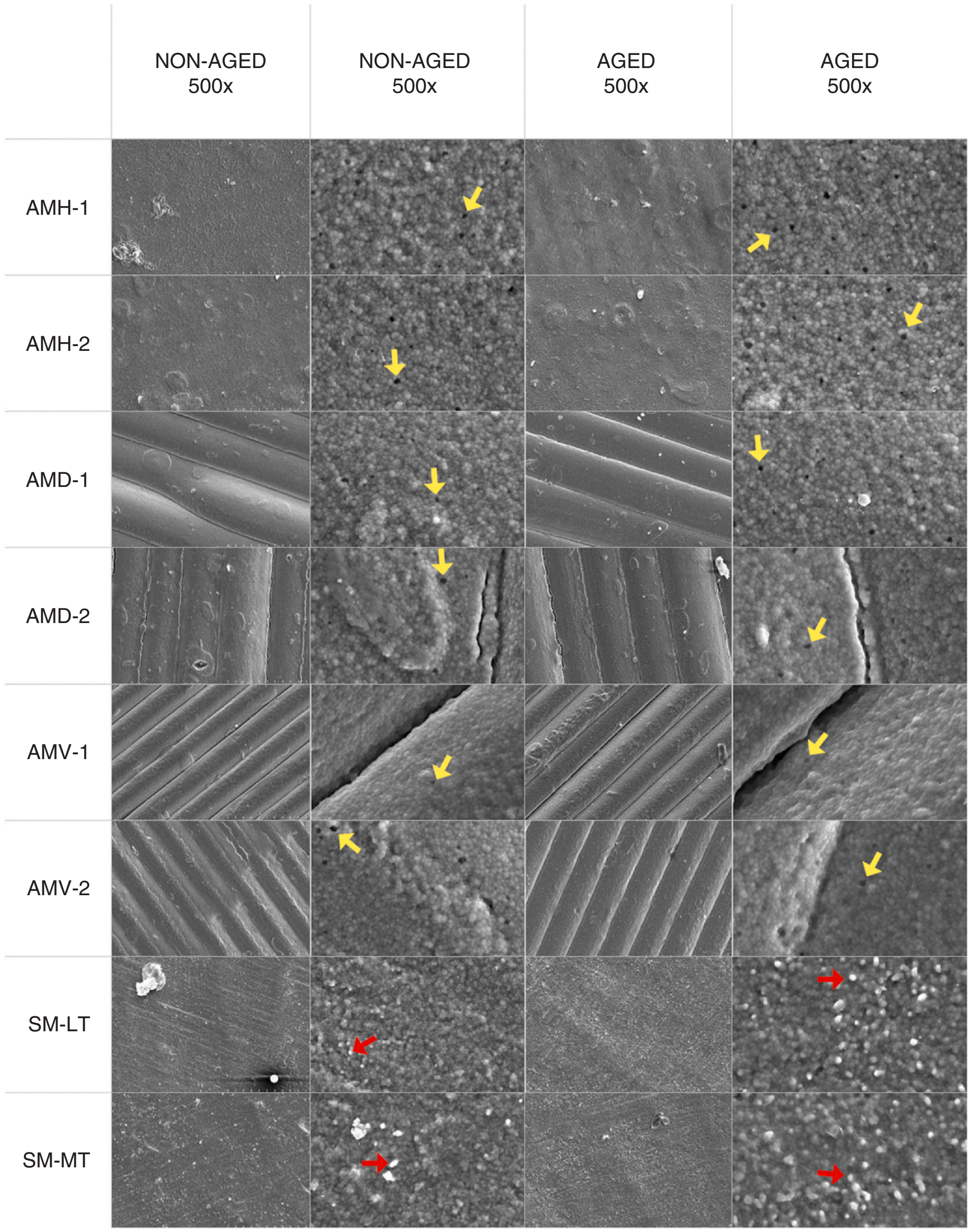

Figure 2. Representative scanning electron microscope images of tested specimens. AMD-1, Additively manufactured zirconia specimens with 45-degree build orientation and 1-step debinding and sintering; AMD-2, Additively manufactured zirconia specimens with 45-degree build orientation and 2-step debinding and sintering; AMH-1, Additively manufactured zirconia specimens with 0-degree build orientation and 1-step debinding and sintering; AMH-2, Additively manufactured zirconia specimens with 0-degree build orientation and 2-step debinding and sintering; AMV-1, Additively manufactured zirconia specimens with 90-degree build orientation and 1-step debinding and sintering; AMV-2, Additively manufactured zirconia specimens with 90-degree build orientation and 2-step debinding and sintering; SM-LT, IPS e.max ZirCAD LT; SM-MT, IPS e.max ZirCAD MT. *Yellow arrows* indicate residual pores and *red arrows* indicate monoclinic-phase zirconia particles.

monolithic prostheses consisting of 4 or more units.[33] In this study, only thermocycled AMV-2 specimens had a mean FS (449 MPa) below the 500 MPa threshold, while AMH-2, SM-LT, and SM-MT specimens showed mean FS values above 800 MPa (821 to 969 MPa) regardless of aging. These findings suggested that the tested materials may be suitable for monolithic fixed partial dentures, with AMH-2, SM-LT, and SM-MT offering greater flexibility for clinicians and dental laboratory technicians by supporting both short- and long-span restorations. Nevertheless, as the aging protocol simulates only a short period of intraoral use,[34] this hypothesis should be further validated through studies assessing the long-term mechanical properties of the tested materials.

XRD and SEM findings contextualize the FS values, as all specimens, regardless of manufacturing method or aging, exhibited distinct tetragonal phase peaks at various 2θ angles and isolated monoclinic peaks at 51.2-degree 2θ. The generally high FS values, mostly exceeding the ISO standard 6872:2024 threshold for 3-unit prostheses,[33] may be attributed to the predominance of the tetragonal phase, the mechanically favorable zirconia form[3] that inhibits crack propagation through transformation toughening.[20,30] Isolated monoclinic peaks indicated tetragonal phase stability under the tested conditions, while delamination and microcracks in AMD and AMV specimens likely contributed to their lower FS by compromising microstructural integrity.[25] Defects observed in both AMD and AMV specimens, regardless of firing process, are potentially associated with build orientation, which has been reported to influence layer number, interlayer bonding quality,[22,28] and the placement of supporting structures during fabrication.[29] Aging influenced the monoclinic phase, critical for stability, mechanical properties, and performance, as tetragonal-to-monoclinic transformation affects toughness and crack resistance. Flexural strength decreased significantly only in AMV-2 specimens, likely because of delamination that became more pronounced after thermocycling. SEM images of AM zirconia revealed pores, particularly in the AMH group; however, AMH specimens exhibited flexural strength comparable with or higher than AMD and AMV specimens across aging conditions, suggesting that porosity was less detrimental than delamination or microcracks. It should be noted that the assessment of pore numbers was based on visual inspection of SEM images and should be confirmed using density measurements or microcomputed tomography analyses. Another notable observation from the SEM images was the presence of monoclinic-phase particles across all materials, with a particularly higher concentration in the SM-LT and SM-MT specimens. XRD diffractograms showed only subtle microstructural changes, whereas SEM images revealed increased size and quantity of monoclinic-phase crystals in SM-LT and SM-MT specimens after thermocycling. Although flexural strength was unaffected, these changes may indicate greater susceptibility to low-temperature degradation, characterized by tetragonal-to-monoclinic transformation in humid environments and known to impair zirconia's mechanical properties.[26]

The build orientations tested in this study were chosen based on their frequent use in previous investigations of 3-point[1,15,16,19,24,32] or biaxial[17,21,28,30,31] FS of AM zirconia. Most studies on 3-point FS reported higher values for specimens printed at 0 degrees,[1,15,16,24,32] except for Coppola et al,[19] who reported higher FS in specimens printed at 90 degrees, potentially because of experimental resins and because the 90-degree specimens were printed along their longitudinal axis (XZ orientation). Two prior studies on biaxial FS using the same 3Y-TZP slurry as in the present study focused either on the combined effects of firing process and build orientation[21] or on the firing process alone.[17] While both studies reported that the firing process did not affect the FS of specimens printed at 90 degrees,[17,21] the study investigating the combined effects found that 0-degree oriented specimens fired with the 1-step process exhibited higher FS than 90-degree oriented specimens fired with either the 1- or 2-step process,[21] differences that may be explained by differences in testing methodologies. Other reports have shown higher biaxial FS values for specimens printed at 0 degrees compared with 45 and 90 degrees,[28,30,31] and some also confirmed the predominance of the tetragonal phase irrespective of build orientation.[1,16,19,28,30]

One zirconia slurry and AM technology were used for AM specimens, and SM specimens were limited to a single brand and milling unit; therefore, the findings should not be generalized to other materials or systems. Standardized layer thickness and build orientation adjustments around a single axis further limit applicability. Although specimen design followed ISO standard 6872:2024[33] for standardization and comparability, it did not replicate the complex geometries of clinical restorations. No polishing or glazing procedures were applied, which may have influenced the results, as surface treatments can substantially affect the mechanical and structural properties of zirconia.[16,24,36,37] Thermocycling was performed without artificial saliva, and no mechanical aging was applied. The absence of a separate sintering step, typically used for external shading in AM zirconia, represents another limitation. Future studies should investigate anatomically shaped prostheses and evaluate fracture toughness, wear resistance, translucency, surface gloss, and color stability after diverse aging protocols to better simulate long-term intraoral behavior and validate these findings, particularly for AM zirconia.

CONCLUSIONS

Based on the findings of this in vitro study, the following conclusions were drawn:

1. The FS of AMH specimens was comparable with that of SM-LT and SM-MT, regardless of firing process or aging. In addition, AMH-2, SM-LT, and SM-MT specimens met the ISO 6872:2024 requirements for monolithic prostheses of 4 or more units, irrespective of aging.
2. Although the tetragonal phase was predominant in all groups, AMD and SM-MT specimens exhibited lower peak intensities than their counterparts produced by the same manufacturing method,

regardless of aging. Aging increased diffraction peak intensities, indicating enhanced local crystallinity across all materials.

3. Observational findings from SEM images showed a more porous structure for AM specimens, regardless of firing process or aging, with XRD indicating higher monoclinic-phase zirconia in SM-LT and SM-MT specimens.

REFERENCES

1. Miura S, Shinya A, Ishida Y, Fujisawa M. Mechanical and surface properties of additive manufactured zirconia under the different building directions. *J Prosthodont Res*. 2022;67:410–417.
2. Van Noort R. The future of dental devices is digital. *Dent Mater*. 2012;28:3–12.
3. Sulaiman TA, Suliman AA, Abdulmajeed AA, Zhang Y. Zirconia restoration types, properties, tooth preparation design, and bonding. A narrative review. *J Esthet Restor Dent*. 2024;36:78–84.
4. Mohammed MK, Alahmari A, Alkhalefah H, Abidi MH. Evaluation of zirconia ceramics fabricated through DLP 3D printing process for dental applications. *Heliyon*. 2024;10:e36725.
5. Hanawa T. Zirconia versus titanium in dentistry: A review. *Dent Mater J*. 2020;39:24–36.
6. Revilla-León M, Meyer MJ, Zandinejad A, Özcan M. Additive manufacturing technologies for processing zirconia in dental applications. *Int J Comput Dent*. 2020;23:27–37.
7. Demirel M, Diken Türksayar AA, Donmez MB, Schimmel M, Yilmaz B. Evaluation of the fabrication trueness and internal fit of additively manufactured two-piece zirconia abutments with different build orientations compared to subtractively manufactured abutments. *J Dent*. 2025;153:105470.
8. Lu Y, van Steenoven A, Dal Piva AMdO, et al. Additive-manufactured ceramics for dental restorations: A systematic review on mechanical perspective. *Front Dent Med*. 2025;6:1512887.
9. Rues S, Zehender N, Zenthöfer A, et al. Fit of anterior restorations made of 3D-printed and milled zirconia: An in-vitro study. *J Dent*. 2023;130:104415.
10. Romario YS, Bhat C, Ramezani M, Pasang T, Chen Z, Jiang C-P. Fabrication of translucent graded dental crown using zirconia-yttrium multi-slurry tape casting 3D printer. *J Mech Behav Biomed Mater*. 2024;152:106406.
11. Alqutaibi AY, Ghulam O, Krsoum M, et al. Revolution of current dental zirconia: A comprehensive review. *Molecules*. 2022;27:1699.
12. Lerner H, Nagy K, Pranno N, Zarone F, Admakin O, Mangano F. Trueness and precision of 3D-printed versus milled monolithic zirconia crowns: An in vitro study. *J Dent*. 2021;113:103792.
13. Revilla-León M, Methani MM, Morton D, Zandinejad A. Internal and marginal discrepancies associated with stereolithography (SLA) additively manufactured zirconia crowns. *J Prosthet Dent*. 2020;124:730–737.
14. Methani MM, Revilla-León M, Zandinejad A. The potential of additive manufacturing technologies and their processing parameters for the fabrication of all-ceramic crowns: A review. *J Esthet Restor Dent*. 2020;32:182–192.
15. Suominen JM, Frankberg EJ, Vallittu PK, et al. Three-dimensional printing of zirconia: Characterization of early stage material properties. *Biomaterial Investigations in Dentistry*. 2019;6:23–31.
16. Xiang D, Xu Y, Bai W, Lin H. Dental zirconia fabricated by stereolithography: Accuracy, translucency and mechanical properties in different build orientations. *Ceram Int*. 2021;47:28837–28847.
17. Zenthöfer A, Schwindling FS, Schmitt C, et al. Strength and reliability of zirconia fabricated by additive manufacturing technology. *Dent Mater*. 2022;38:1565–1574.
18. Branco A, Silva R, Santos T, et al. Suitability of 3D printed pieces of nanocrystalline zirconia for dental applications. *Dent Mater*. 2020;36:442–455.
19. Coppola B, Schmitt J, Lacondemine T, Tardivat C, Montanaro L, Palmero P. Digital light processing stereolithography of zirconia ceramics: Slurry elaboration and orientation-reliant mechanical properties. *J Eur Ceram Soc*. 2022;42:2974–2982.
20. Alhotan A, Yilmaz B, Weber A, Babaier R, Bourauel C, Fouda AM. Effect of artificial aging on fracture toughness and hardness of 3D-printed and milled 3Y-TZP zirconia. *J Prosthodont* 2024.
21. Zenthöfer A, Ilani A, Schmitt C, Rammelsberg P, Hetzler S, Rues S. Biaxial flexural strength of 3D-printed 3Y-TZP zirconia using a novel ceramic printer. *Clin Oral Investig*. 2024;28:145.
22. Branco AC, Colaço R, Figueiredo-Pina CG, Serro AP. Recent advances on 3D-printed zirconia-based dental materials: A review. *Materials (Basel)*. 2023;16:1860.
23. Sim J-H, Koo B-K, Jung M, Kim D-S. Study on debinding and sintering processes for ceramics fabricated using digital light processing (DLP) 3D printing. *Processes*. 2022;10:2467.
24. Lu Y, Wang L, Dal Piva AMdO, et al. Influence of surface finishing and printing layer orientation on surface roughness and flexural strength of stereolithography-manufactured dental zirconia. *J Mech Behav Biomed Mater*. 2023;143:105944.
25. Puchakayla PKR, Pegu B, Gandhi P, Singh G. Defects evolution during printing, debinding and sintering for additive manufacturing of yttria stabilized zirconia. *Mater Charact* 2025:114752.
26. Zhai Z, Sun J. Research on the low-temperature degradation of dental zirconia ceramics fabricated by stereolithography. *J Prosthet Dent*. 2023;130:629–638.
27. Sabatini GP, Çakmak G, Kahveci Ç, Al-Johani H, Yilmaz B, Dönmez MB. Surface roughness, stainability, and translucency of additively manufactured zirconia with different build orientations and firing processes after coffee thermocycling. *J Prosthet Dent*. 2025;134:830.e1–830.e8.
28. Osman RB, van der Veen AJ, Huiberts D, Wismeijer D, Alharbi N. 3D-printing zirconia implants; a dream or a reality? An in-vitro study evaluating the dimensional accuracy, surface topography and mechanical properties of printed zirconia implant and discs. *J Mech Behav Biomed Mater*. 2017;75:521–528.
29. Mou Z, Zhong J, Wang F, et al. Zirconia crowns manufactured using digital light processing: Effects of build angle and layer thickness on the accuracy. *J Dent*. 2024;151:105359.
30. Abualsaud R, Abussaud M, Assudmi Y, et al. Physiomechanical and surface characteristics of 3D-printed zirconia: An in vitro study. *Materials (Basel)*. 2022;15:6988.
31. Hetzler S, Hinzen C, Rues S, Schmitt C, Rammelsberg P, Zenthöfer A. Biaxial flexural strength and vickers hardness of 3D-printed and milled 5Y partially stabilized zirconia. *J Funct Biomater*. 2025;16:36.
32. Marsico C, Øilo M, Kutsch J, Kauf M, Arola D. Vat polymerization-printed partially stabilized zirconia: Mechanical properties, reliability and structural defects. *Addit Manuf*. 2020;36:101450.
33. International Organization of Standardization. ISO 6872. Dentistry — Ceramic materials. Geneva: ISO,; 2024⟨https://www.iso.org/obp/ui/en/#iso:std:iso:6872:ed-5:v1:en⟩.
34. Gale M, Darvell B. Thermal cycling procedures for laboratory testing of dental restorations. *J Dent*. 1999;27:89–99.
35. Sabatini GP, Yoon H-I, Çakmak G, Al-Haj Husain N, Yilmaz B, Dönmez MB. Mechanical properties and reliability of an additively manufactured resin incorporated with a commercially available ceramic composite concentrate. *J Prosthet Dent*. 2025;133:1089.e1–1089.e7.
36. Lu Y, Wang L, Dal Piva AMdO, et al. Effect of printing layer orientation and polishing on the fatigue strength of 3D-printed dental zirconia. *Dent Mater*. 2024;40:190–197.
37. Silva S, Silva B, Crispim AHT, Dal Piva AMO, Kleverlaan CJ, Souza R. Effect of different finishing/polishing techniques and glaze application on the flexural strength of ultratranslucent zirconia after hydrothermal aging. *J Mech Behav Biomed Mater*. 2025;164:106924.
38. Nakai H, Inokoshi M, Nozaki K, et al. Additively manufactured zirconia for dental applications. *Materials (Basel)*. 2021;14:3694.
39. Abualsaud R, Abussaud M, Assudmi Y, et al. Physiomechanical and surface characteristics of 3D-printed zirconia: An in vitro study. *Materials (Basel)*. 2022;15:6988.

Corresponding author:
Dr Mustafa Borga Dönmez
Department of Reconstructive Dentistry and Gerodontology
School of Dental Medicine
University of Bern
Freiburgstrasse 7
Bern 3010
SWITZERLAND
Email: mustafa-borga.doenmez@unibe.ch

Acknowledgments
This study was funded by the Buser Implant Foundation Junior Investigator Grant (Grant Number: JIG 24-03).

https://doi.org/10.1016/j.prosdent.2025.10.043